INSTITUTE OF PLASMA PHYSICS

NAGOYA UNIVERSITY

Ion Beam - Plasma Interaction at Right Angles to the External Magnetic Field

Y. Kiwamoto,* M. Inutake and Y. Kita

IPPJ-257 August 1976

RESEARCH REPORT

NAGOYA, JAPAN

Ion Beam - Plasma Interaction at Right Angles to the External Magnetic Field

Y. Kiwamoto,* M. Inutake and Y. Kita

IPPJ-257 August 1976

Further communication about this report is to be sent to the Research Information Center, Institute of Plasma Physics, Nagoya University, Nagoya, Japan.

Permanent Address: Research Institute for Energy Materials, Yokohama National University, Yokohama, Japan

Abstract

Lower hybrid wave instability caused by the interaction between a plasma and an ion beam perpendicular to an external magnetic field is studied both theoretically and experimentally. A homogeneous magnetized plasma with large volume and an ion beam source with large cross section [20 cm × 100 cm] have been constructed for this purpose. We report observations of the wave propagation and the relaxation of the ion beam distribution, and discuss the effect of the magnetic field which deforms the distribution into a stable form.

§1. Introduction

A study of the interaction between a plasma and an ion beam injected at right angles to the external magnetic field is very important for the realization of the neutral-beam= injection heating of the large-scale Tokamak plasma.[1,2] When the beam propagates obliquely to the magnetic field or when there is no magnetic field, the electrons make an ion-acoustic response to the beam. The resultant ion-acoustic turbulence has been studied extensively and understood very well.[3-6] However when the beam propagates almost at right angles to the magnetic field and if the electron motion along the wave electric field is inhibited, the way of the beam-plasma interaction should be quite different.[7,8] A theoretical study indicates that in this case a new instability appears which is supported by lower hybrid mode waves.

Such a plasma configuration may be realized in other fields; for example in the interaction between the magnetosphere plasma and the impinging high energy solar ion beams[9] and in the collision of the high speed shock front with the unheated rest plasma ions of theta pinch experiments.[10] In spite of the importance of the instability only a little has been understood. In order to make an explicit experiment on this problem, a homogeneous magnetized plasma with large volume is needed. For this purpose we constructed a linear machine which contains two magnetized plasmas of large volume and with good uniformity. In the course of this work we found a similar work of R. P. H. Chang[8] who had constructed essentially the same type of machine and studied the same

problem. However, our results are somewhat different both theoretically and experimetally. The details of the theoretical work will be published elsewhere. In the present paper, the first phase of our experimental work is reported. In section 2 we describe the characteristics of the experimental device and the plasma. A theoretical consideration is made in section 3. Section 4 is devoted to the experiemtal studies on the wave propagation and the ion beam relaxation. A discussion is made in section 5.

§2. Production of large magnetized palsma

We divide the cylindrical volume of a vacuum chamber [32 cm in dia. × 150 cm in length] axially into two hemicircular cylinders by a fine stainless steel mesh. As shown in Fig.1, a plasma is produced by a steady discharge in one part. The wall of the vacuum chamber serves as an anode. Inside the counterpart, an inner chamber made of stainless steel, electrically insulated from the vacuum chamber wall, is mounted and produces an electrically independent plasma which serves as an ion beam source. The space potentials of the two plasmas are determined by the potentials of the anode walls. When a potential difference is applied between the anodes, ions are injected to the plasma with lower space potential.[11] The electron motion along the beam is inhibited by the external magnetic field produced by four pancake coils 40 cm apart from each others. The axial inhomogeneity of the magnetic field is about 10 percent peak to peak.

In order to confine the primary electrons and increase the plasma homogeneity, the multipole magnetic structure is

formed at all ends of the plasma column[12] with ceramic permanent magnets. The maximum strength of the magnetic field of the multipole is about 1.5 kgauss which is much stronger than that in the plasma volume [$\lesssim$ 200 gauss] but decreases rapidly into the plasma. The surfaces of the permanent magnets are covered with thin stainless stell sheets or thin aluminum foils so as not to be deteriorated by the radiation from the incandescent filaments.

Each cathode consists of ten thoriated tungsten filaments [0.3 mm in diam. and 10 cm in length] oriented perpendicularly to the magnetic field. Two ways of alignment of the filaments are examined. When the filaments are set perpendicular to the direction of the beam which is injected horizontally [x - axis], the floating potential varies spatially by an amount of 15 V peak to peak [upper trace in Fig.2]. The distributions of the ion saturation current and the electron saturation current are shown in lower traces in Fig.2. In spite of the large variation of the floating potential which is sensitive to the flux of the primary electrons emitted from the filaments, the space potential lies within the limits of 1 V around +4 V with respect to the anode potential. When the filaments are set parallel to the beam, the variation of the space potential is reduced by a factor of 2, while the variation of the floating potential is not reduced appreciably as shown in the top trace of Fig.3. The distribution of the plasma density is also plotted in the middle portion of Fig.3 [when the beam is not injected] and the lower portion of the same figure [when the beam is injected with energy of 15 eV].

The magnetic field is varied as a parameter. The radial density distribution of the magnetized plasma is satisfactorily homogeneous. In the following experiment we adopt the latter filament configuration. The measurements on two probes 40 cm apart axially [z - direction] indicate that the plasma is almost homogeneous along the axis at least in the scale of the probe separation.

The plasma parameters are as follows: the electron temperature $T_e \simeq 5$ eV, the background ion temperature $T_i \simeq 0.5$ eV, the plasma density $n_p = (1\text{-}5) \times 10^{10}$ cm^{-3}, the argon gas pressure $p = (1\text{-}5) \times 10^{-4}$ Torr. The magnetic field B is varied from 50 gauss to 200 gauss. The effective temperature of the beam ions is highly anisotropic; the perpendicular temperature $T_{b\perp}$ does not appreciably change from the background temperature T_i but the paralle temperature $T_{b\parallel}$ is much smaller than T_i due to the potential acceleration of the beam. Some remarks are made in the discussion.

Spontaneous density fluctuations are observed below 10 kHz. Although the noise level is not low [$\delta n/n_0 \simeq 0.1$], we consider the noise will not appreciably affect the propagation of lower hybrid waves with much higher frequency and short wavelength.

§3. Theory of ion-ion two stream instability

The linear dispersion relation of the perpendicular ion-ion two-stream system is made briefly in this section. We consider waves whose frequencies lie in the range $\omega_{ci} << \omega << \omega_{ce}$, where ω_{ci} and ω_{ce} stand for the ion and electron

cyclotron frequency, respectively; i.e. while electrons are fully magnetized, ions are not.

From the linearized collisionless Boltzmann equation we obtain the following dispersion relation[8)]

$$1 + \frac{\omega_{pe}^2}{\omega_{ce}^2}\left(\frac{k_\perp}{k}\right)^2 - (1-\eta)\frac{T_e}{2T_i}\left(\frac{k_D}{k}\right)^2 Z'\left(\frac{\omega}{k v_i}\right)$$

$$-\eta\frac{T_e}{2T_b}\left(\frac{k_D}{k}\right)^2 Z'\left(\frac{\omega - \mathbf{k}\cdot\mathbf{U}}{k v_b}\right) - \frac{1}{2}\left(\frac{k_D}{k}\right)^2 Z'\left(\frac{\omega}{k_z v_e}\right) = 0 \quad , \qquad (1)$$

where η is the beam density fraction [$\eta = n_b/n_p$], k_D^{-1} and ω_{pe} are the electron Debye length and electron plasma frequency, respectively. The components of the wave vector $\mathbf{k}$ are defined as $k_z = (\mathbf{k}\cdot\mathbf{B})/B$, $k_\perp = (k^2 - k_z^2)^{1/2}$. All the quantities are projected to the direction of the wave vector $\mathbf{k}$. Therefore the temperatures T_e, T_i and T_b [electron, background ion and beam ion, respectively] mean effective values in this direction; v_e, v_i and v_b are associated thermal velocities. The function $Z(\zeta)$ is the plasma dispersion function. If we neglect the terms of order m_e/m_i [mass ratio], using the normalized frequency and wavenumber $\bar{\omega} = \omega/\omega_{LH} = \omega(1 + (\omega_{pe}/\omega_{ce})^2)^{1/2}/\omega_{pi}$, $\bar{k} = k(1 + (\omega_{pe}/\omega_{ce})^2)^{1/2}/k_D$, we can reduce eq.(1) to

$$1 - (1-\eta)\frac{T_e}{2T_i}\frac{1}{\bar{k}^2}Z'\left(\frac{c_s}{v_i}\frac{\bar{\omega}}{\bar{k}}\right)$$

$$-\eta\frac{T_e}{2T_b}\frac{1}{\bar{k}^2}Z'\left(\frac{c_s}{v_b}\frac{\bar{\omega}}{\bar{k}} - \frac{\mathbf{k}\cdot\mathbf{U}}{\bar{k}\,v_b}\right) - \frac{1}{2\bar{k}^2}Z'\left(\frac{1}{\sqrt{2}\,\theta}\frac{\bar{\omega}}{\bar{k}}\right) = 0 \quad , \qquad (2)$$

where $c_s = \sqrt{T_e/m_e}$, $\theta = (k_z/k)(m_i/m_e)^{1/2}$.

Mapping of the contour $\mathrm{Im}\bar{\omega} = 0$ onto the complex plane corresponding to the left hand side of eq.(2) indicates that the number of the mode which has positive imaginary $\bar{\omega}$ is zero or one.[13] The unstable solution appears essentially due to the reactive interaction between the lower hybrid waves supported by the two groups of the ions[14] [two-stream instability]. Although eq.(2) has many stable solutions we restrict our attention to four modes which exist even in the hydrodynamic limit. One of the four modes propagates in the opposite direction to the beam so that it should not appear in the experiment. The remaining three modes are plotted in Fig.4. The lower hybrid wave 1 belonging to the background ion is unstable when θ is small [$\lesssim 0.7$], while the slow beam mode 2 becomes unstable when θ is larger. In both cases it is not the resonant electrons but the reactive interaction between two waves which drives the instability.[8] When the propagation angle θ is appreciably larger than 1, the growth rate diminishes rapidly into negative value, and the lower hybrid wave changes continuously to an ion acoustic wave.[8]

It should be noted that the growth rate is considerably larger $\gamma \sim 0.2\omega_{LH}$. The maximum growth rate with implicit parameter k is shown in Fig.5. The range of θ and the value of the maximum growth rate increase with the beam velocity u [Fig.5(a)]. Its dependence on the beam temperature T_b is shown in Fig.5(b). As the beam temperature increases the

range of θ and the maximum growth rate decreases. In the maximum-growth-rate diagram we do not have any peak around $\theta = 1$, in contrast with the results of R. P. H. Chang.[8] It will be found later that the linear stability analysis shown in Fig.5 is essential for the examination of the wave growth even in the nonlinear stage, because the beam distribution spatially changes independently of the turbulence. The analysis shown in Fig.5 does not change with T_e/T_i, so long as the beam density fraction η is small. This is because the phase velocity of the unstable wave is considerably larger than the background ion thermal velocity, and the ion Landau damping is weak.

§4. Experiment

4.1 Test wave propagation

We examine the dispersion relation of the wave in the perpendicular ion beam-plasma system. The propagation of test waves, which are launched by slightly modulating the beam velocity, is observed by the interferometric technique. Concentrating our attention to the waves with frequency around the lower hybrid frequency where the growth rate is expected to be the largest, we plot the interferometric traces of the test waves in Fig.6.

When the magnetic field B is 150 gauss we observe the waves to grow weakly. The spatial growth rate is estimated to be $k_i \approx 0.7\ \mathrm{cm}^{-1} \lesssim 0.1\ k_r$, where k_i, k_r stand for the imaginary part and the real part of the wave vector $k_\perp$. In terms of the temporal growth rate we find $\gamma \lesssim 0.1\ \omega_{LH}$. This

value is smaller than the expected maximum growth rate by a factor of 3.

The linear theory indicates that the waves are unstable when their phase velocities along the magnetic field are sufficiently greater than the electron thermal velocity. Because the maximum wavelength along the magnetic field is geometrically bounded, the above requirement imposes that the lower hybrid frequency, which is roughly proportional to the magnetic field strength, should be sufficiently high. This explains why the waves do not grow when B is less than 150 gauss.

On the other hand, when the magnetic field is much stronger, we do not observe growing test waves. This may be attributed to the rapid deformation of the beam velocity distribution into a stable shape by the strong Lorentz force, which will be considered later.

The experimental dispersion relations are plotted in Fig.7. We find that the phase velocities of the test waves are less than but close to the beam velocity. Comparison with the theoretical disperison relation indicates that the angle parameter θ is larger than 1, say 3. This means that the parallel wavelength is less than the plasma length and comparable with the distance between the adjacent pancake coils. As shown in Fig.5, in this range of θ, the growth rate of the test wave is so small that the collision between the ions and the neutral atoms easily quenches the instability.

4.2 Velocity distribution of beam ions

The amplitude of the growing test wave does not keep the same value after its saturation but damps away so quickly that it cannot be explained in terms of the ion-neutral collision frequency [Fig.6]. The heavy damping of the test wave is attributable to the strong wave-particle interaction.

The spatial evolution of the ion velocity distribution function is plotted in Fig.8(a). As the beam propagates in the x direction, the peak of the distribution shifts downward and the width increases. The deformation of the distribution leads to an increase of the resonant beam ions which cause strong Landau damping of the test waves.

In the experiment on the unmagnetized ion beam instability, similar features were observed and they were attributed to nonlinear wave-particle interactions in the ion acoustic wave turbulence.[3,5] In the present experiment, however, the fluctuation amplitude of the lower hybrid wave is so small [$\delta n/n_0 < 10^{-2}$] that the deformation of the velocity distribution cannot be attributed to the wave-particle interaction.

This supposition is supported by the observation of the temporal evolution of the distribution at a fixed point x = 5 cm [Fig.9]. The ion beam is switched on at t = 0 and switched off at t = 70 μsec. Because the distribution does not change noticeably during the time while the ion beam exists [from 20 μsec to 90 μsec], we conclude that the distribution does not change by the wave-particle interaction.

We then examine the effect of the magnetic field on the

distribution. We observe the change of the distribution at a fixed position as the magnetic field is increased with the initial beam energy kept constant. Figure 10 shows the distribution at x = 6 cm. It is now clear that the deformation of the beam distribution shown in Fig.8(a) is due to the Lorentz force of the magnetic field. In the next section we compare the observed distribution with the theoretical one for which only the Lorentz force is considered.

§5. Discussion

5.1 Growth rates of unstable waves

In the experiment of the test wave propagation, the growth rates of the waves were found to be less than 0.1 ω_{LH}. Since the beam density fraction is kept at 0.1, the observed growth rate is smaller than the theoretical maximum growth rate by a factor of 3. In the experiment of R. P. H. Chang, the both growth rates agreed very well.[8)]

Figure 5 suggests that the apparent discrepancy can be attributed to the value of θ which is not actually small in the experiments. In order to determine the value of θ experimentally, the interferometric trace of the test wave propagation along the magnetic field is necessary. However, since the wavelength parallel to the field is very long, the experimental determination is difficult, and no experimental data have been obtained yet. The shortest characteristic length along the field of the plasma is about 40 cm determined by the spacing of the magnetic field coils. If we let the parallel half wavelength to be 40 cm, the typical value of θ

in our argon plasma is 2.5, the linear dispersion relation well explains the small experimental growth rates.

Then if we decrease the parameter θ below 1, strong lower hybrid wave turbulence should be generated. Since the value k_z/k is geometrically bounded, it may be the most effective to change the ion species to lighter ones. We shall study the lower hybrid turbulence in a hydrogen plasma in the next stage of the experiment.

5.2 Velocity distribution of beam ion

Special attentions should be paid to the unperturbed change of the velocity distribution of the beam ions in the magnetic field. In the acceleration stage of the ion beam, the velocity distribution becomes anisotropic.[3,5] Because of the Lorentz force exerted perpendicularly to the beam direction, the beam trajectory changes as it propagates into the target plasma, and the initial anisotropy spreads the velocity distribution projected to the initial direction [x - axis]. In this subsection we compare the observed distribution with the theoretical one derived from the stationary unperturbed collisionless Boltzmann equation.

$$v_x \frac{\partial}{\partial x} f(\mathbf{v}, x) + \frac{e}{m_i c} [\mathbf{v} \times \mathbf{B}] \cdot \frac{\partial}{\partial \mathbf{v}} f(\mathbf{v}, x) = 0 \quad . \tag{3}$$

Imposing the boundary condition at x = 0

$$f(\mathbf{v}, 0) = A_0 f(v_z) \exp\left\{ - \frac{(v_x - u)^2}{a_x^2} - \frac{v_y^2}{a_y^2} \right\} \quad , \tag{4}$$

we obtain the distribution at $x > 0$

$$f(\mathbf{v},x) = A_0 f(v_z)\exp\left\{-\frac{\left[(v_x^2 - 2x\omega_c v_y - x^2\omega_c^2)^{\frac{1}{2}} - u\right]^2}{a_x^2} - \frac{(v_y^2 + x\omega_c)^2}{a_y^2}\right\} \qquad (5)$$

Here, a_x and a_y are the thermal velocity in the x and y direction, respectively. The derivation of (5) is shown in Appendix. Normalizing the distance and the velocity as $x\omega_c/a_y = X$, $v_x/a_y = V_x$, and $u/a_y = U$, we obtain the projected velocity distirubiton function

$$f(V,X) = \frac{A_0 a_y}{X}\int_0^\infty d\zeta\, \zeta \exp\left\{-\left(\frac{a_y}{a_x}\right)^2(\zeta - U)^2 - \frac{(\zeta^2 - V_z^2 - X^2)^2}{4X^2}\right\} \qquad (6)$$

This function has a peak at $V_{xo} = (U^2 - X^2)^{1/2}$.

We first consider the shift of the peak in the distribution. The normalized kinetic energy V_{xo}^2/U^2 is plotted in Fig.11(a). Here experimental values of ω_c and u used in Fig.8(a) are introduced. In order to fit the observed distribution to the theoretical curve, we must shift the origin $x = 0$ into the source plasma by an amount of δ. The optimum value of δ is 4 cm.

We then consider the width of the distribution. The spatial change of the effective thermal velocity $\Delta(V_x^2)/4V_{xo}$, where $\Delta(V_x^2)$ is the full width at the half maximum of $V_x^2 - f(V_x,X)$ distribution, is plotted by the solid line in Fig.11 (b) as a function of anisotropy index $(a_y/a_x)^2$. The experimental values processed in the same way from Fig.8(a) are plotted with correction δ. Here the experimental value T_i = 0.5 eV has been used.

From the comparison between the experimental data and

the theoretical values, we find that the distribution (6) represents the observed velocity distribution pretty well. Figure 8(b) shows the theoretically expected distribution function with the assumption $(a_y/a_x)^2 = 500$, $\delta = 4$ cm.

These values give some informations about the beam source plasma. If the ion temperature before the acceleration is T_0, the parallel beam temperature after the acceleration $T_{b\parallel}$ is approximately $T_0^2/2mu^2$. Since the perpendicular temperature does not change by the acceleration, the anisotropy parameter $(a_y/a_x)^2$ should be equal to $2mu^2/T_0$. In order to meet the expected value 500 when $mu^2/2 = 50$ eV, the ion temperature of the beam source should be $T_0 \simeq 0.4$ eV; this value is quite reasonable in the present experiment. The value of δ indicates that the accelerating plasma double layer exists not at the plasma boundary but in the source plasma. It lies around the sheet of the lines of force of the magnetic field which pass the cathode filament nearest to the separating metal mesh.

Note that the abscissa is scaled as v^2 in both figures in Fig.8. The almost symmetric shape of the distribution with respect to the peak is the characteristic feature which is not observed in the ion beam turbulence in unmagnetized plasmas.[3-5)]

Since the beam distribution deforms without the excitation of unstable waves, the unstable test waves always damp away beyond some critical distance which is mainly determined by the magnetic field strength and the beam velocity. In the present experiment the characteristic distance is

approximately 0.1 u/ω_c. When we analyze the turbulent relaxation of the distribution in the experiments in future, careful considerations of this process are indispensable.

§6. Conclusion

In this paper a theoretical study of the lower hybrid instability caused by the perpendicular ion beam in a magnetized plasma was briefly presented. A large-volume homogeneous magnetized plasma was produced in order to study experimentally the instability. Multipole magnetic configuration at the plasma ends was found to be effective to make the plasma homogeneous. The test wave propagation showed that there exists an unstable wave near the lower hybrid frequency. But because of the finite parallel wavelength imposed by the inhomogeneity of the magnetic field, the angle parameter θ was larger than 1 and the growth rate was appreciably smaller than the maximum growth rate. This may be overcome in the future experiment by changing the mass ratio m_i/m_e to smaller one. Stabilizing effect of the magnetic field through the Lorentz force was pointed out. The observed ion velocity distribution agreed well with the theoretical one determined by the stationary Boltzmann equation combined with the appropriate boundary conditions, which in turn informs us of the way of the ion beam formation.

Acknowledgements

The authors employed the vacuum chamber which had previously been prepared by Dr. H. Ikezi for the study of the

Langmuir wave soliton. They thank to Dr. A. Ishida of Niigata University for a stimulating discussion. They appreciate the continuous interest and encouragement of Prof. K. Takayama. One of the author (Y.K.) would like to thank Prof. H. Tanaca of Yokohama National University for his support.

Appendix

The motion of the ion corresponding to the collisionless Boltzmann equation (3) is described by

$$\frac{d\mathbf{V}}{dt} = \frac{e}{m_i c}\left[\mathbf{V} \times \mathbf{B}\right] . \tag{A.1}$$

We solve this equation in the x-y plane imposing the boundary condition that at $t = t_0$, $x = 0$ and $v_\perp = (v_{xo}, v_{yo}) = (v_\perp\cos\phi, v_\perp\sin\phi)$. Then we obtain

$$\begin{aligned} v_x &= v_\perp \cos\left[-\omega_c(t-t_0) + \phi\right] \\ v_y &= v_\perp \sin\left[-\omega_c(t-t_0) + \phi\right] \end{aligned} \tag{A.2}$$

and

$$\chi = -\frac{v_\perp}{\omega_c}\left\{\sin\left[-\omega_c(t-t_0)+\phi\right] - \sin\phi\right\} . \tag{A.3}$$

Solving (A.2) and (A.3) inversely we find

$$\begin{aligned} v_{x0} &= v_\perp\cos\phi = \left[v_x^2 - 2\chi\omega_c v_y - \chi^2\omega_c^2\right]^{\frac{1}{2}} \\ v_{y0} &= v_\perp\sin\phi = v_y + \chi\omega_c . \end{aligned} \tag{A.4}$$

If we introduce these equations into (4), we obtain the final result (5).

References

1) H. P. Furth, Nuclear Fusion 15 (1975) 487.

2) H. L. Berk, W. Horton, Jr., M. N. Rosenbluth and P. H. Rutherford, MATT-1127 (1975).

3) R. J. Taylor and F. V. Coronitti, Phys. Rev. Letters 29 (1972) 34.

4) D. R. Baker, Phys. Fluids 16 (1973) 1730.

5) Y. Kiwamoto, J. Phys. Soc. Japan 37 (1974) 466.

6) F. Doveil and D. Grésillon, Phys. Fluids 18 (1975) 1756.

7) K. Papadopoulos, R. C. Davidson, J. M. Dawson, I. Haber, D. A. Hammer, N. A. Krall and R. Shanny, Phys. Fluids 14 (1971) 849.

8) R. P. H. Chang, Phys. Rev. Letters 35 (1975) 285.

9) T. Obayashi, Solar Terrestrial Physics, (Syōkabō Press, Tokyo 1970).

10) H. Itô, S. Gotô, H. Kishimoto, N. Satomi, M. Ushio and T. Uyama, (1974) IAEA-CN-33/E8-5, Tokyo.

11) R. J. Taylor, K. R. MacKenzie and H. Ikezi, Rev. Sci. Instrum. 43 (1972) 1675.

12) E. R. Ault and K. R. MacKenzie, Rev. Sci. Instrum. 44 (1973) 1697.

13) A. B. Mikhailovskii, Theory of Plasma Instability Vol.1 (Consultants Bureau, New York 1974).

14) A. Ishida and K. Nishikawa, to be published in J. Phys. Soc. Japan.

Figure Captions

Fig.1 The experimental apparatus. Ion beam with cross section of 20 cm × 100 cm is injected to the target plasma with effective volume 20 cm × 15 cm × 110 cm.

Fig.2 Radial distributions of the floating potential and the ion and electron saturation currents when the filaments are set perpendicular to the beam. Plasma space potential lies within the limits of 1 V.

Fig.3 Radial distributions of the floating potential [top trace], ion saturation currents without the beam [middle traces], and ion saturation currents with the beam [15 eV] injected [lower traces], when the filaments are set parallel to the beam. Plasma space potential lies within the limits of 0.5 V.

Fig.4 Dispersion relation of the waves in the ion beam= plasma system. Parameters are: (a) $\eta = 0.1$, $T_e/T_i = 10$, $T_e/T_b = 10$, $u/c_s = 3$, $\theta = 0.5$, (b) $\eta = 0.1$, $T_e/T_i = 10$, $T_e/T_b = 10$, $u/c_s = 3$, $\theta = 1$. Solid lines represent the real part, dots the imaginary part.

Fig.5 Maximum growth rate vs. angle parameter $\theta = (k_z/k)(m_i/m_e)^{1/2}$. Parameters are $\eta = 0.1$, $T_e/T_i = 10$. u/c_s is varied in Fig.5(a) with $T_e/T_b = 10$ fixed. T_e/T_b is varied in Fig.5(b) with $u/c_s = 3$ fixed.

Fig.6 Propagation of the test waves with frequency around $\omega_{LH}/2\pi$. $\eta = 0.1$, $T_e/T_i = 10$ and $\frac{1}{2}mu^2 = 40$ eV.

Fig.7 Dispersion relation of the test waves.

Fig.8 (a) Observed velocity distribution of the beam ion.

(b) Calculated velocity distribution of the beam ion.

Fig.9 Temporal evolution of the ion velocity distribution at x = 5 cm. B = 100 gauss. The beam is turned on at t = 0 and turned off at t = 70 μsec.

Fig.10 The ion velocity distribution at x = 6 cm. The strength of the magnetic field is varied.

Fig.11 (a) Shift of the peak of the beam distribution. Solid line represents the theoretical one. Experimental values are plotted for various δ. δ = 1 cm, 2 cm, 4 cm for ○, △, □, respectively.

(b) Evolution of the effective thermal velocity. Best fitting is made when δ = 4 cm, $(a_y/a_x)^2 = 500$.

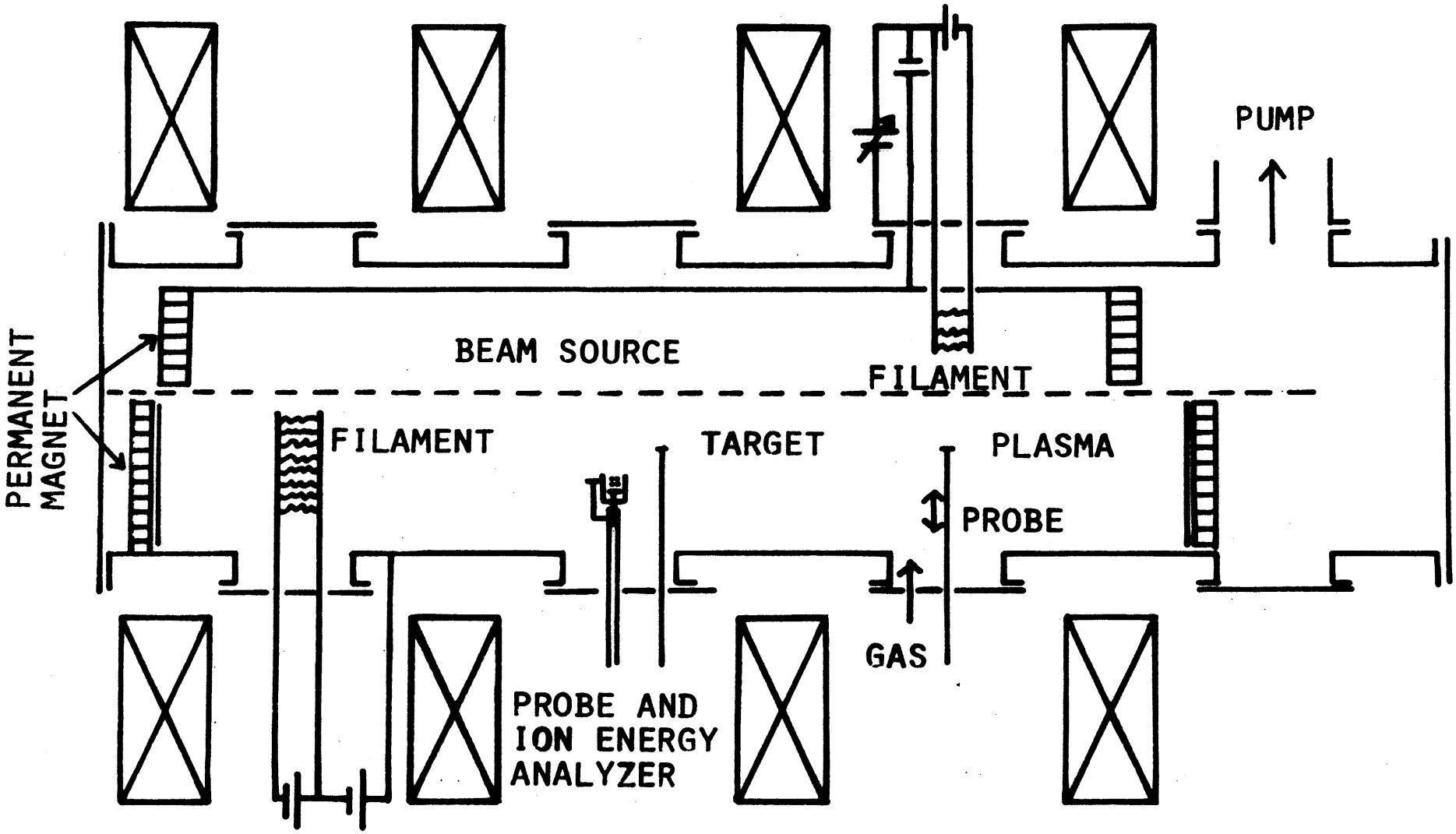
PUMP
BEAM SOURCE
FILAMENT
PERMANENT MAGNET
FILAMENT
TARGET
PLASMA
PROBE
GAS
PROBE AND ION ENERGY ANALYZER

Fig. 1

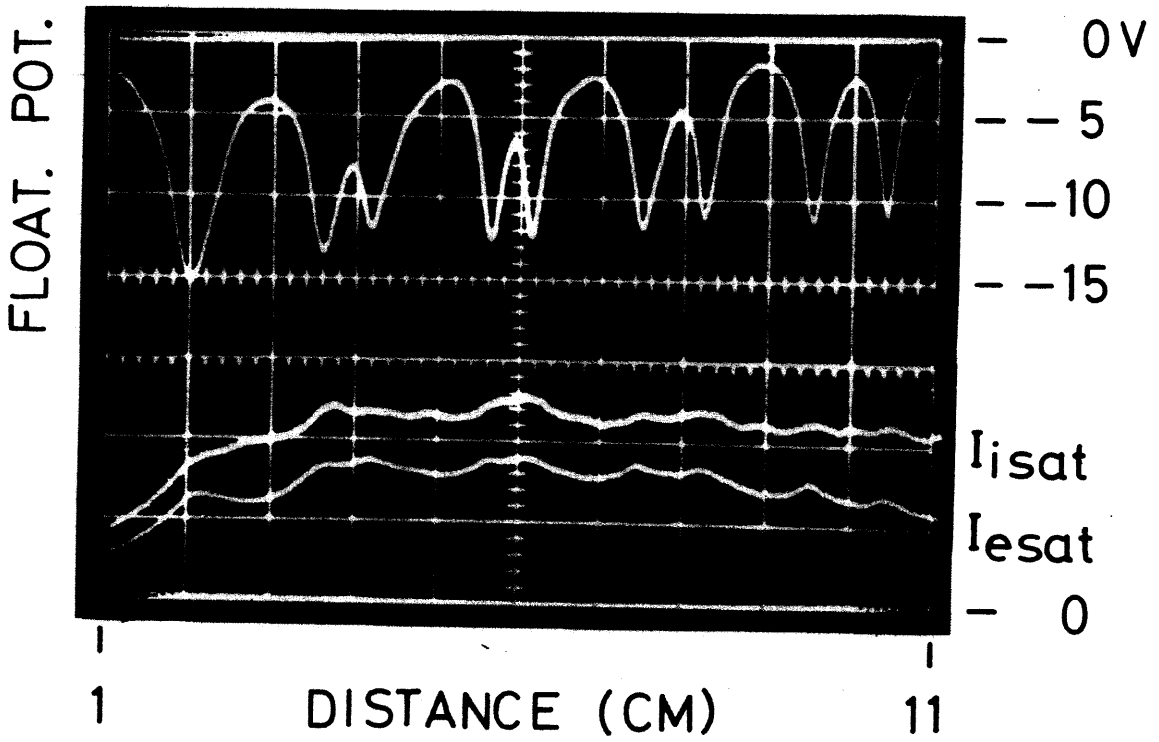

Fig. 2

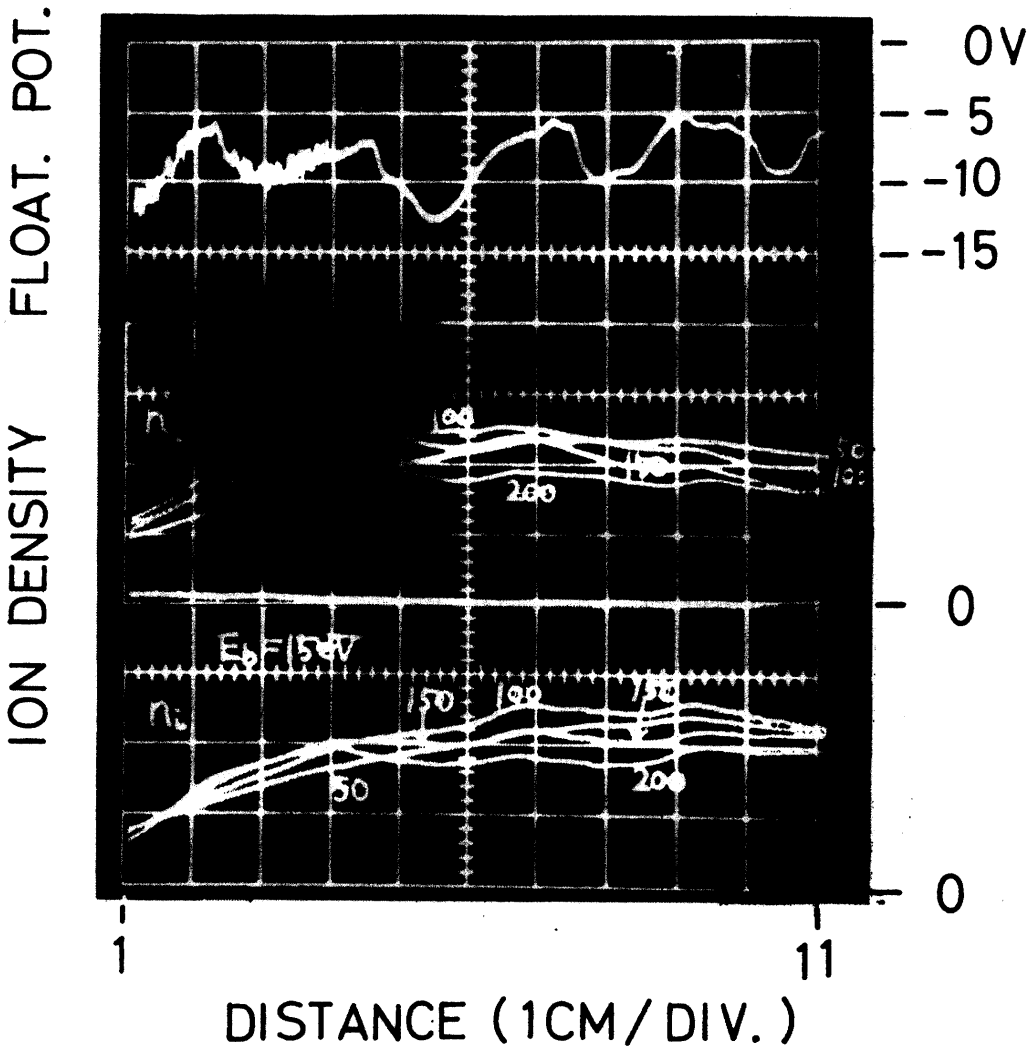

Fig. 3

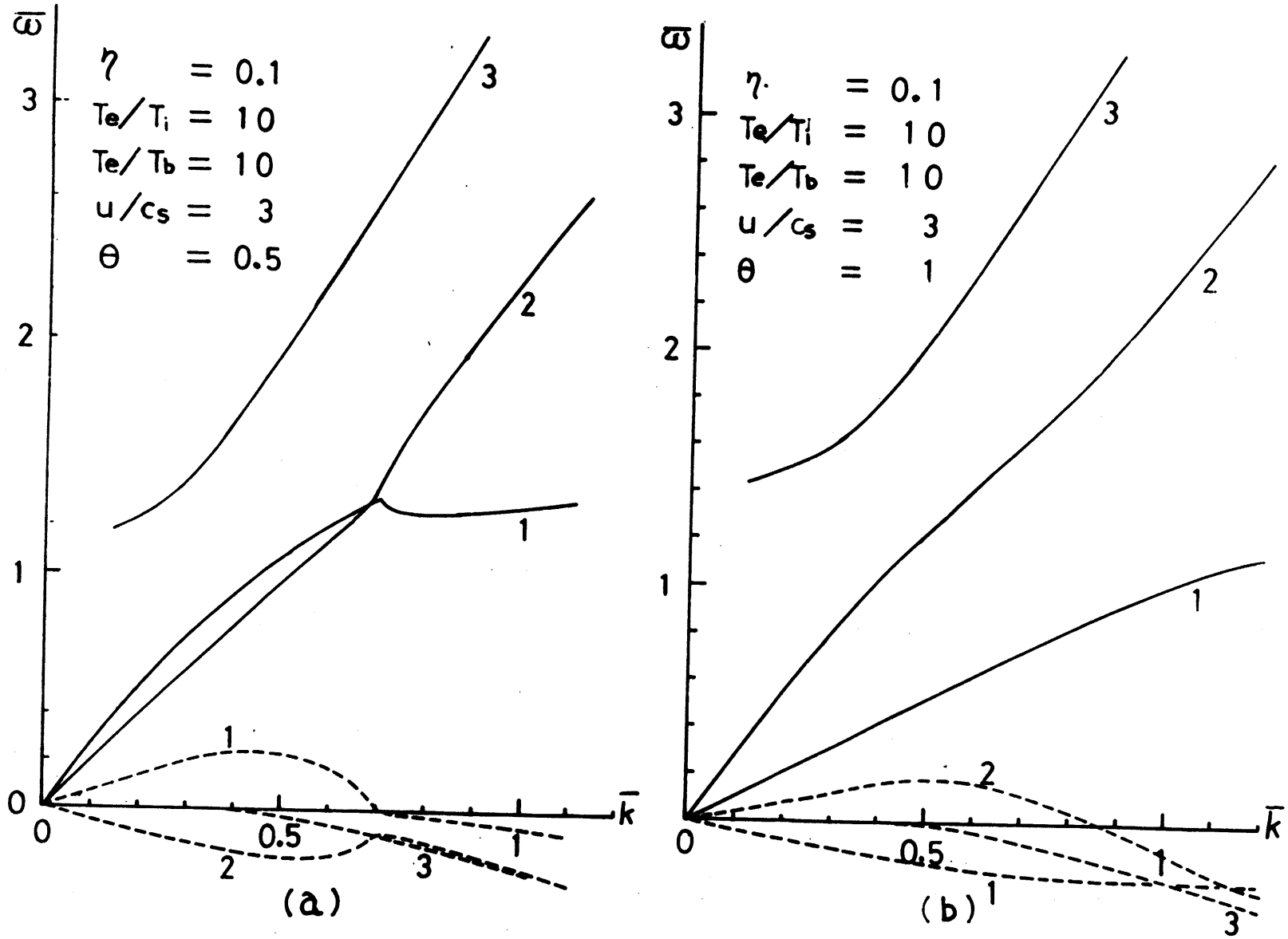
ω̄
η = 0.1
Te/Ti = 10
Te/Tb = 10
u/cs = 3
θ = 0.5
3
2
1
0
0
0.5
1
k̄
1
2
3
(a)
ω̄
η = 0.1
Te/Ti = 10
Te/Tb = 10
u/cs = 3
θ = 1
3
2
1
0
0.5
1
k̄
1
2
3
(b)

Fig. 4

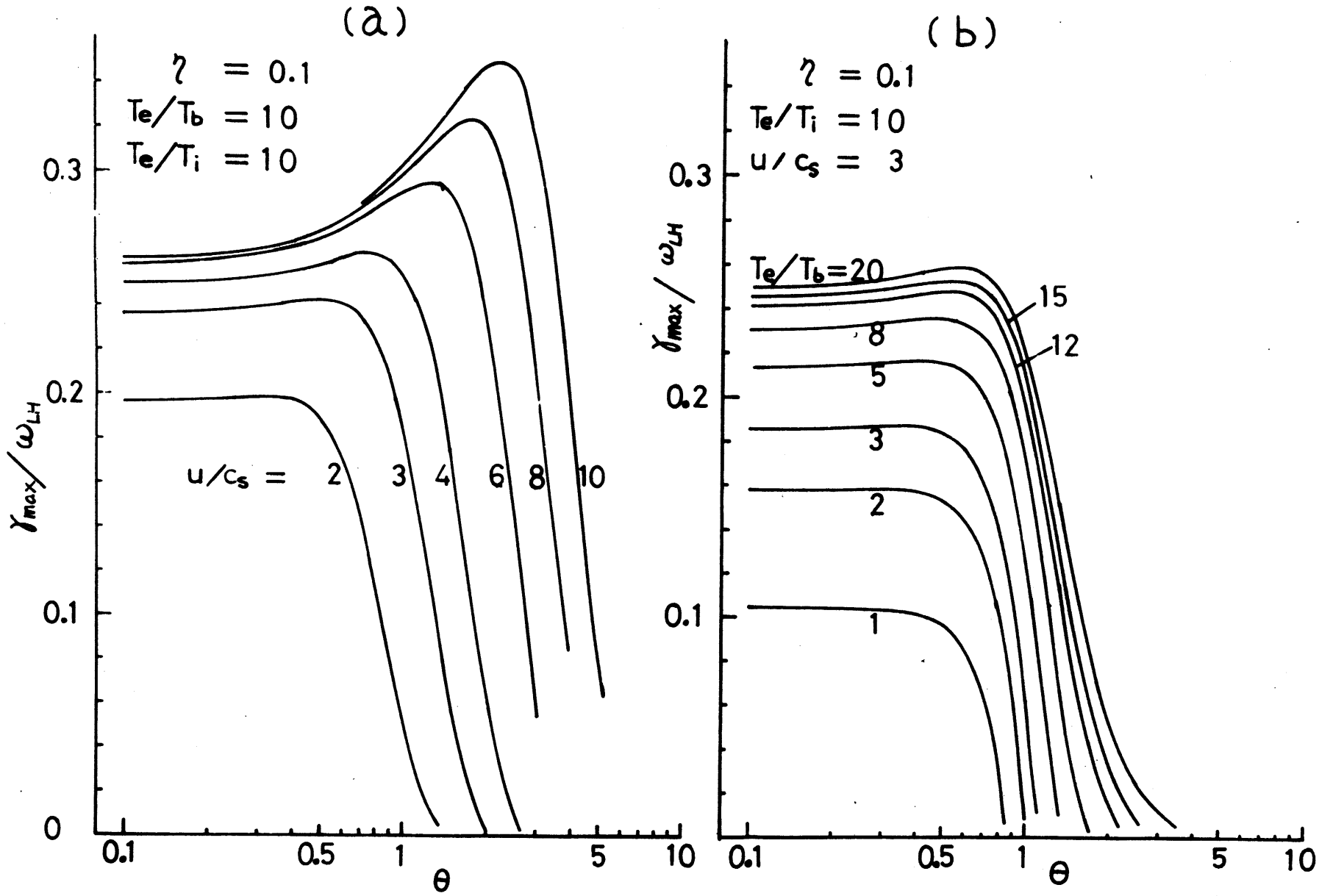
(a)
η = 0.1
Te/Tb = 10
Te/Ti = 10
u/cs = 2 3 4 6 8 10
γmax/ωLH
0.3
0.2
0.1
0
0.1
0.5
1
5
10
θ
(b)
η = 0.1
Te/Ti = 10
u/cs = 3
Te/Tb=20
15
12
8
5
3
2
1
γmax/ωLH
0.3
0.2
0.1
0.1
0.5
1
5
10
θ

Fig. 5

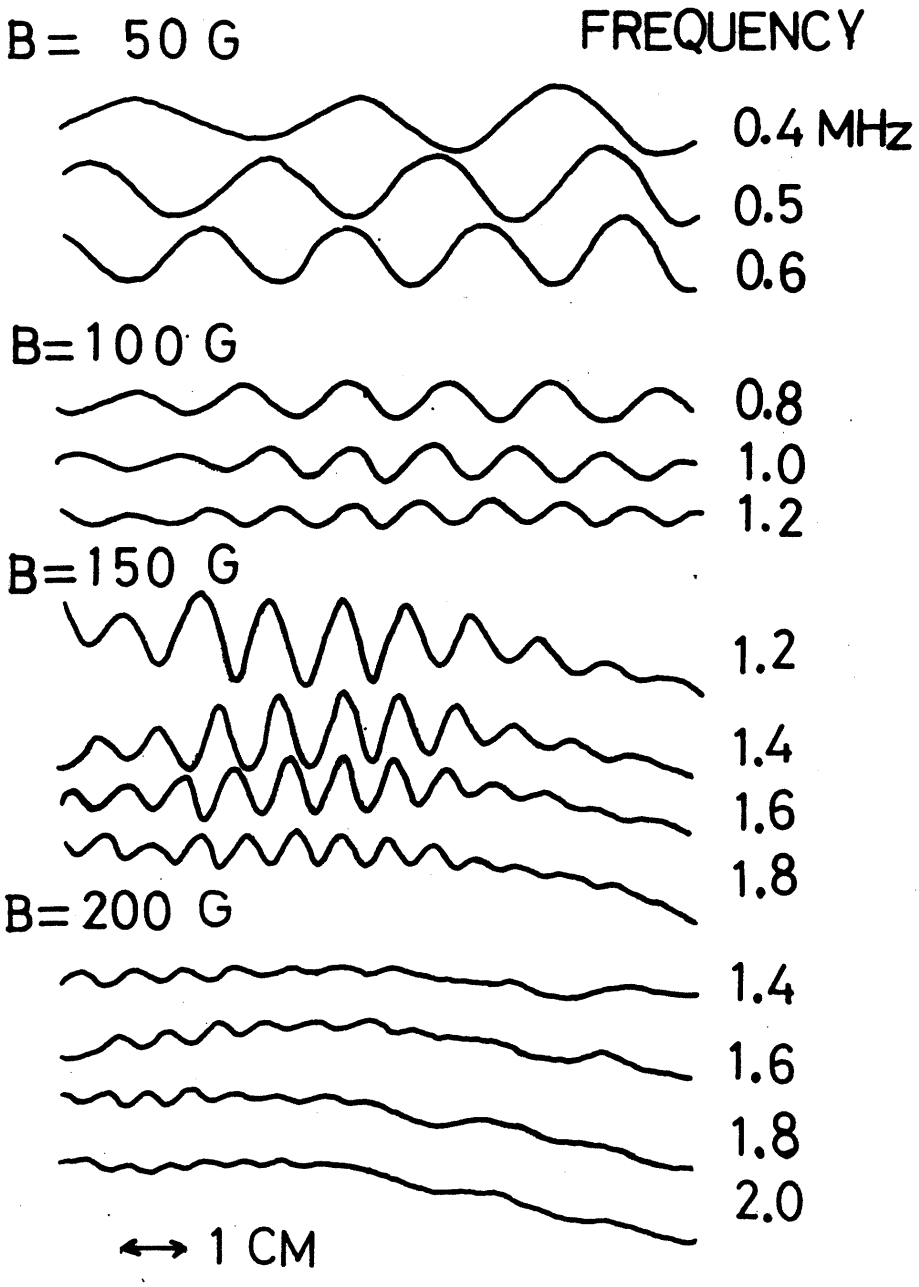
B= 50 G
FREQUENCY
0.4 MHz
0.5
0.6
B=100 G
0.8
1.0
1.2
B=150 G
1.2
1.4
1.6
1.8
B=200 G
1.4
1.6
1.8
2.0
1 CM

Fig 6

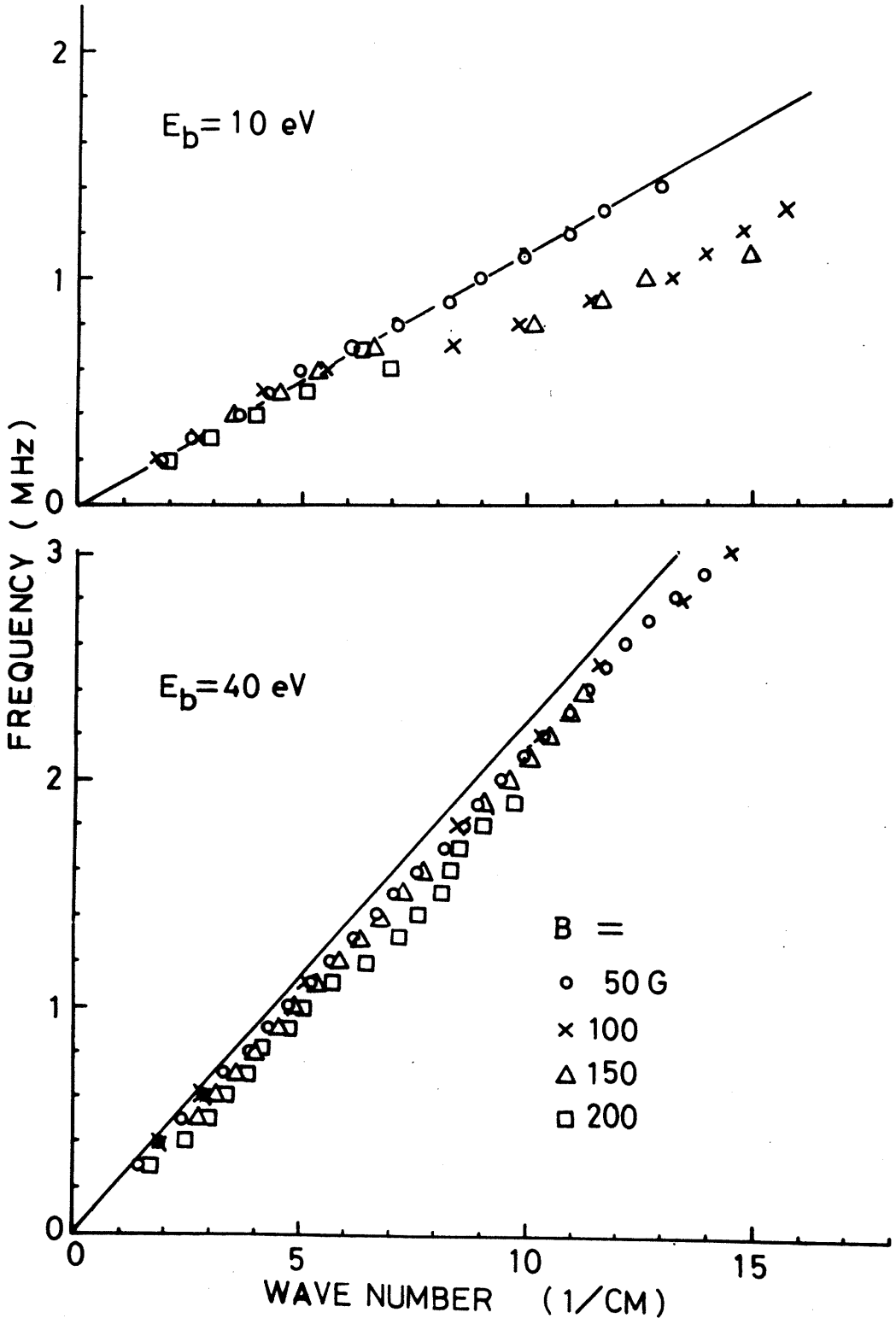
E_b= 10 eV
E_b=40 eV
FREQUENCY (MHz)
WAVE NUMBER (1/CM)
B =
o 50 G
× 100
△ 150
□ 200
0
1
2
3
5
10
15

Fig. 7

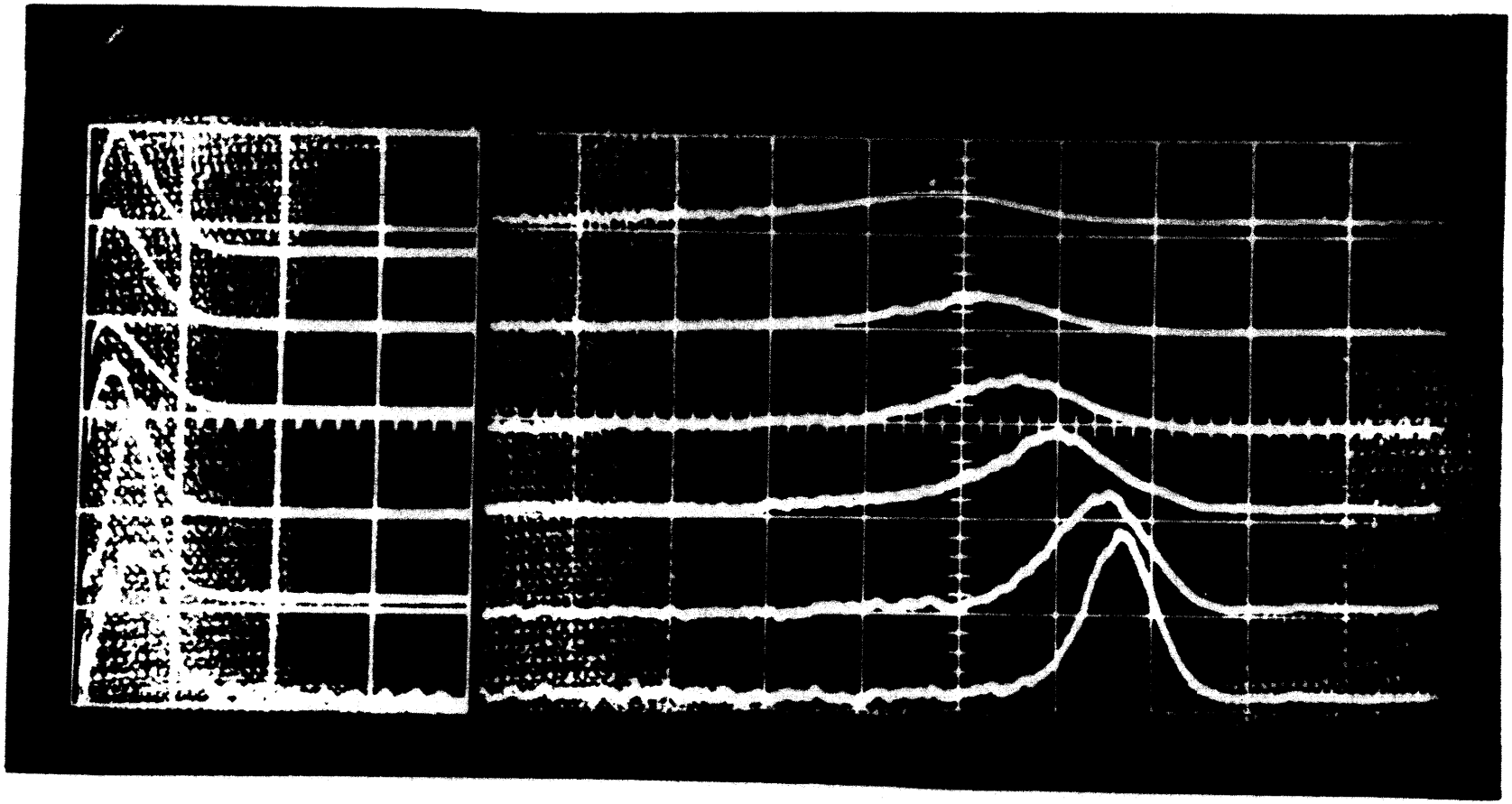

Fig. 8(a)

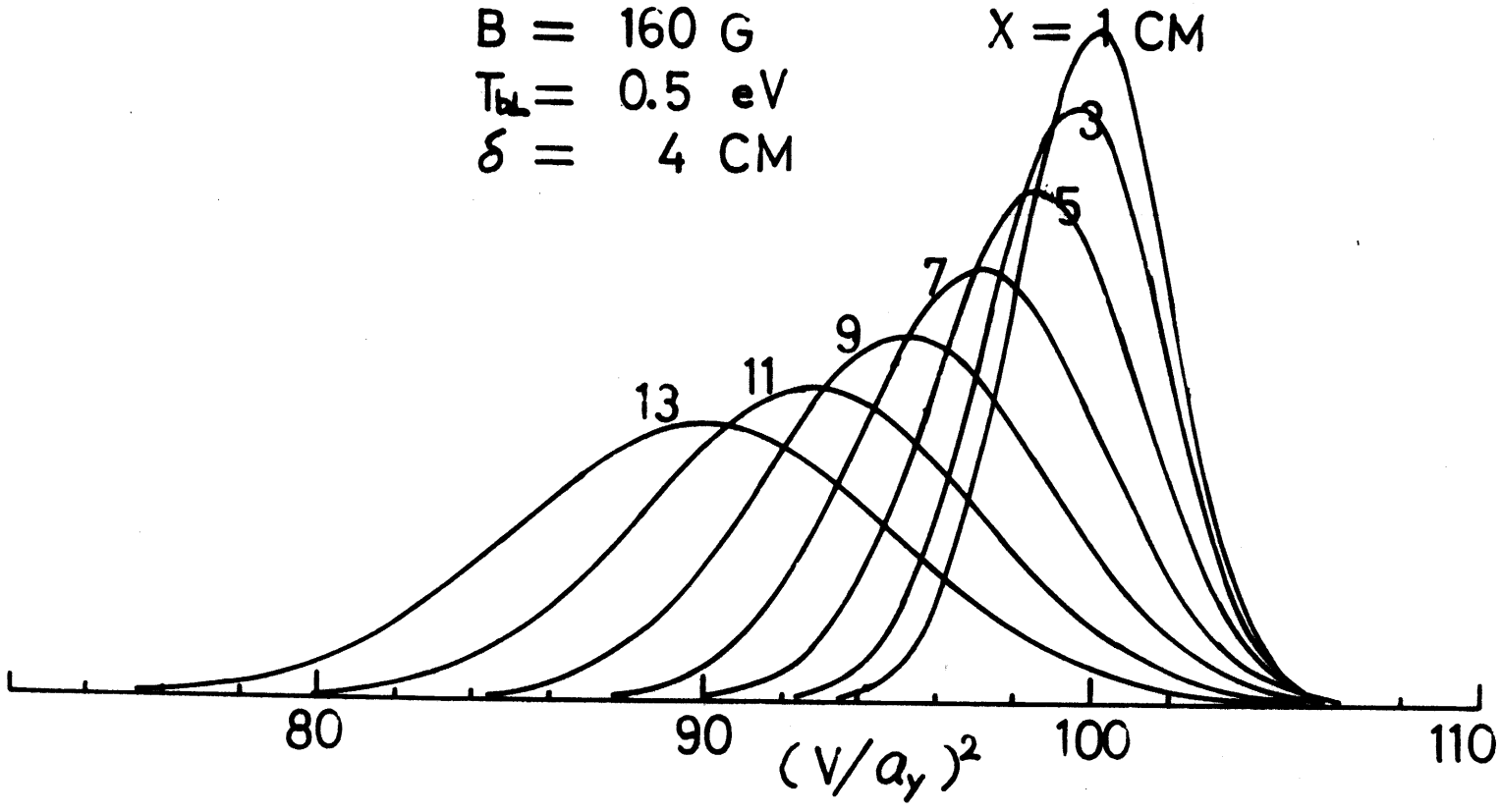

Fig. 8(b)

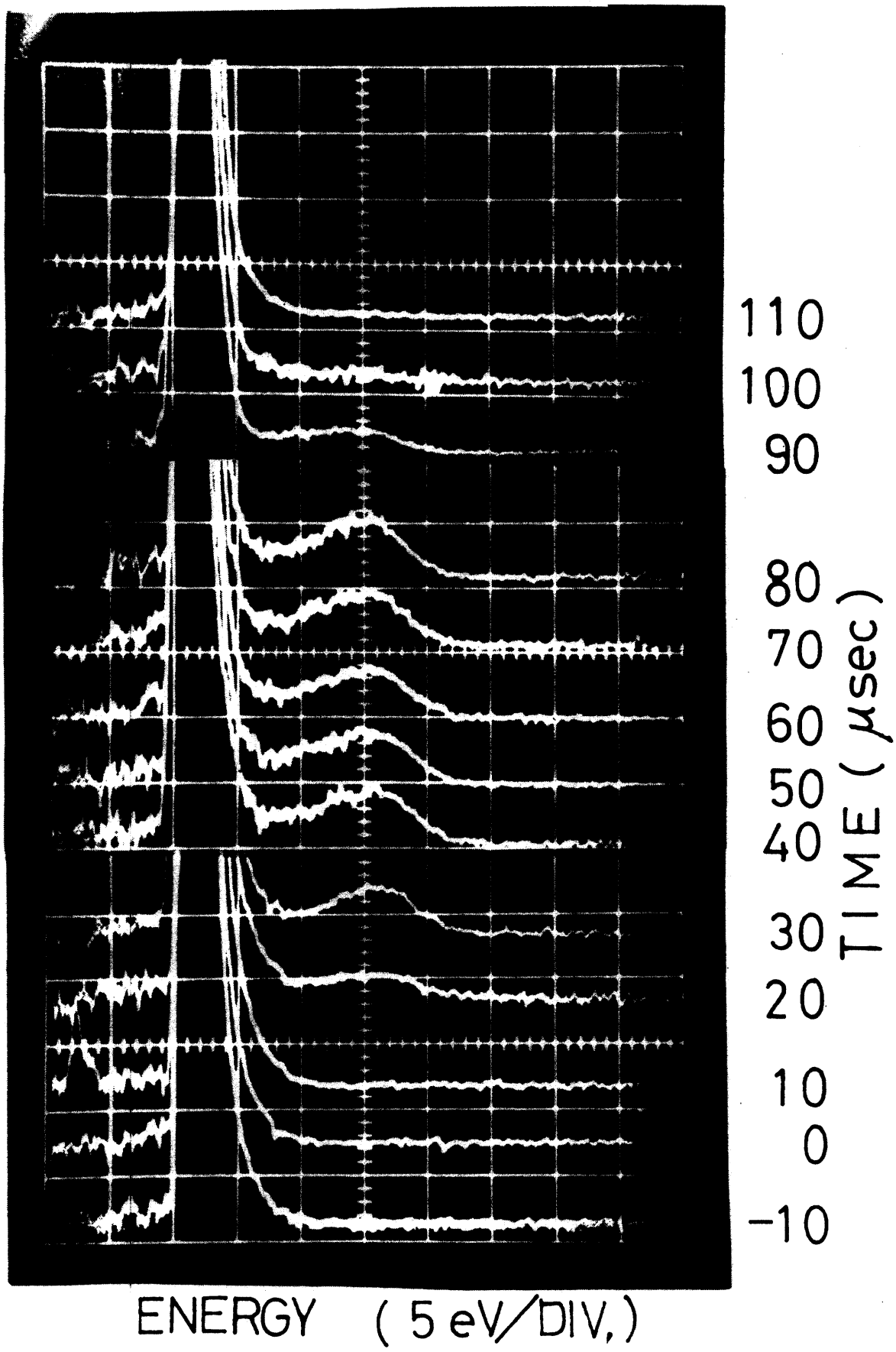

Fig. 9

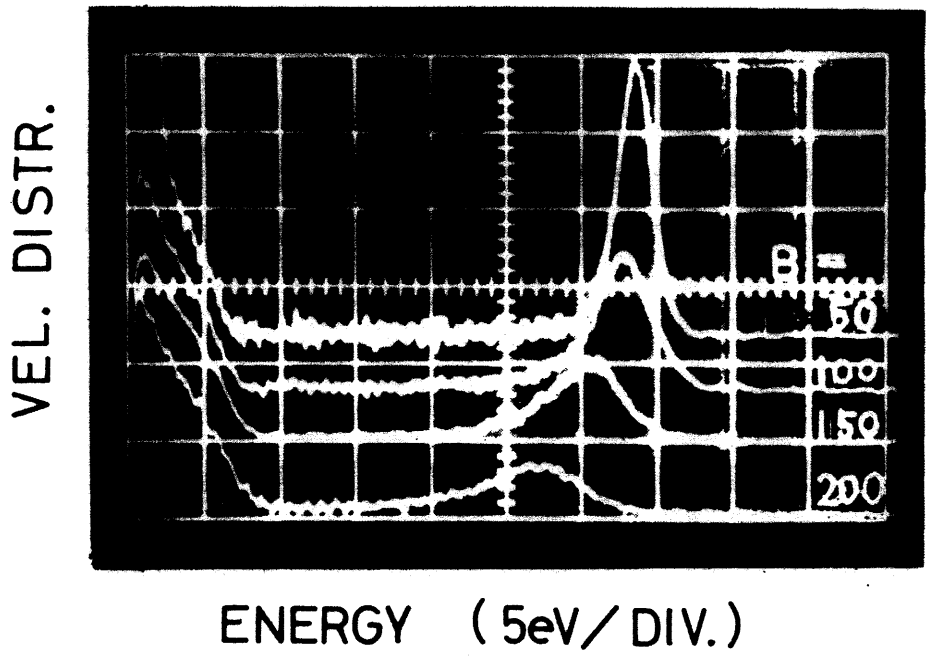

Fig. 10

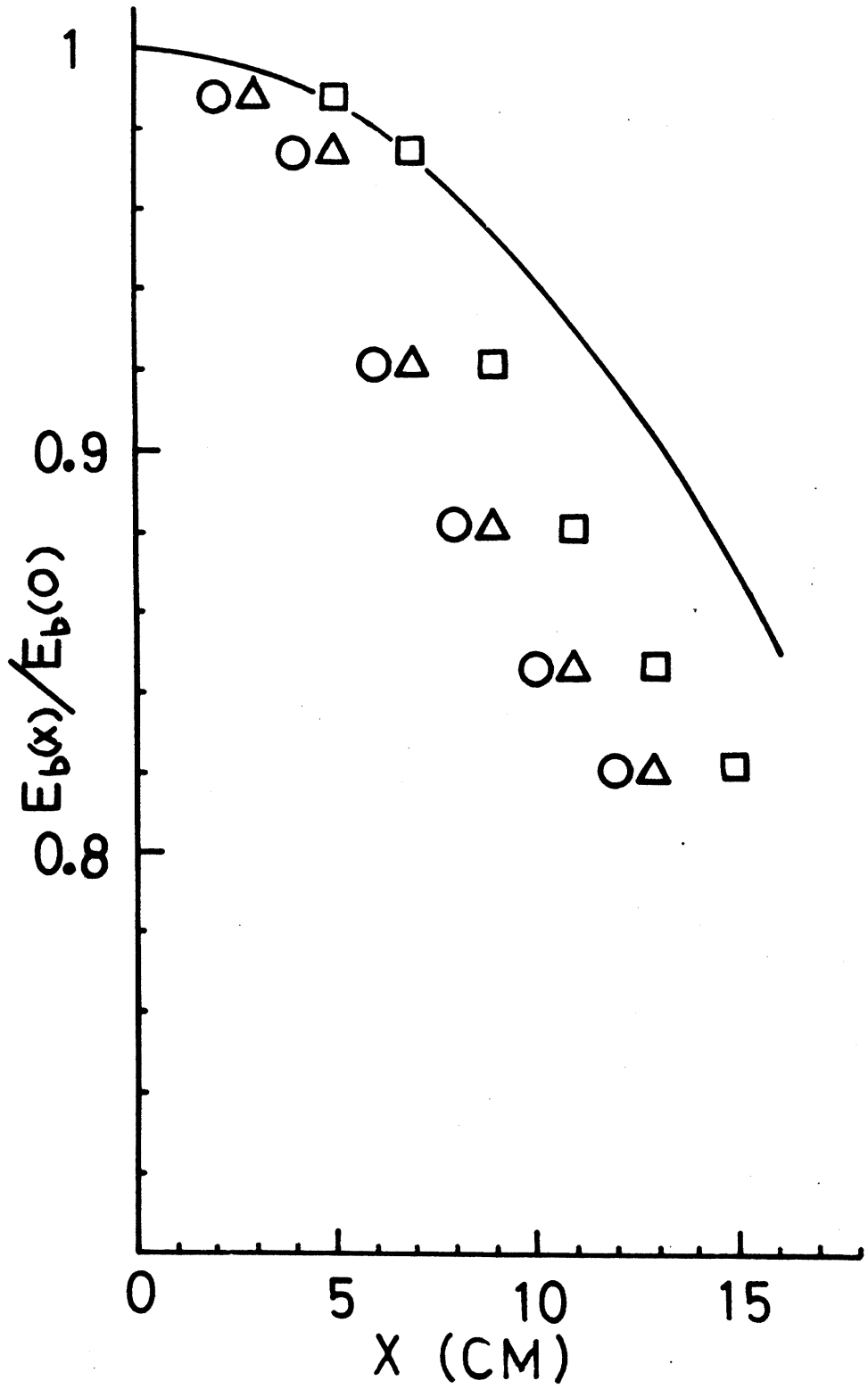

Fig. 11(a)

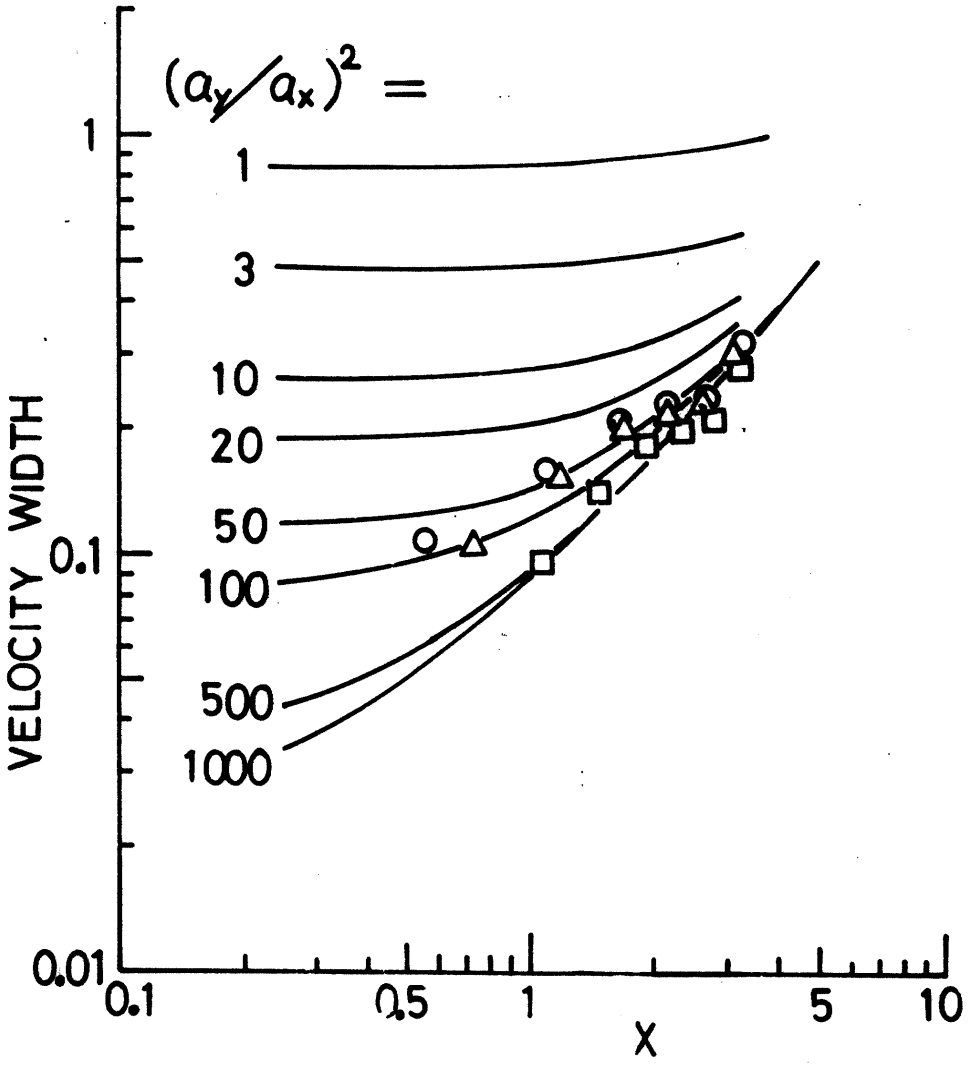
$(a_y/a_x)^2$ =
1
3
10
20
50
100
500
1000
VELOCITY WIDTH
1
0.1
0.01
0.1
0.5
1
5
10
X

Fig. 11(b)